


Article

Single Ventricle Reconstruction III: Brain Connectome and Neurodevelopmental Outcomes: Design, Recruitment, and Technical Challenges of a Multicenter, Observational Neuroimaging Study

Vanessa Schmithorst ¹, Rafael Ceschin ^{1,2}, Vincent Lee ¹, Julia Wallace ¹, Aurelia Sahel ¹, Thomas L. Chenevert ³ , Hemant Parmar ³, Jeffrey I. Berman ⁴, Arastoo Vossough ⁴ , Deqiang Qiu ⁵, Nadja Kadom ⁵, Patricia Ellen Grant ⁶ , Borjan Gagoski ⁷, Peter S. LaViolette ⁸ , Mohit Maheshwari ⁸, Lynn A. Sleeper ^{9,10}, David C. Bellinger ¹¹, Dawn Ilardi ¹², Sharon O'Neil ¹³, Thomas A. Miller ¹⁴, Jon Detterich ¹⁵ , Kevin D. Hill ¹⁶, Andrew M. Atz ¹⁷, Marc E. Richmond ¹⁸, James Cnota ¹⁹ , William T. Mahle ²⁰, Nancy S. Ghanayem ^{21,22}, J. William Gaynor ²³, Caren S. Goldberg ²⁴, Jane W. Newburger ⁹ , and Ashok Panigrahy ^{1,*} 

- ¹ Department of Radiology, UPMC Children's Hospital of Pittsburgh, 4401 Penn Avenue, Floor 2, Pittsburgh, PA 15224, USA
- ² Department of Biomedical Informatics, University of Pittsburgh School, 5607 Baum Blvd., Pittsburgh, PA 15206, USA
- ³ Michigan Medicine Department of Radiology, University of Michigan, 1500 E Medical Center Dr., Ann Arbor, MI 48109, USA
- ⁴ Department of Radiology, Children's Hospital of Philadelphia, 3401 Civic Center Blvd., Philadelphia, PA 19104, USA
- ⁵ Department of Radiology and Imaging Sciences, Children's Healthcare of Atlanta, Emory University, 1364 Clifton Rd, Atlanta, GA 30322, USA
- ⁶ Children's Hospital Boston, Fetal-Neonatal Neuroimaging and Developmental Science Center (FNNDSC), 300 Longwood Avenue, Boston, MA 02115, USA
- ⁷ Department of Radiology, Children's Hospital Boston, 300 Longwood Avenue, Boston, MA 02115, USA
- ⁸ Department of Radiology, Medical College of Wisconsin, 9200 W Wisconsin Avenue, Milwaukee, WI 53226, USA
- ⁹ Department of Cardiology, Boston Children's Hospital, 300 Longwood Avenue, Boston, MA 02115, USA
- ¹⁰ Department of Pediatrics, Harvard Medical School, 25 Shattuck Street, Boston, MA 02115, USA
- ¹¹ Cardiac Neurodevelopmental Program, Department of Neurology, Boston Children's Hospital, 300 Longwood Avenue, Boston, MA 02115, USA
- ¹² Department of Neuropsychology, Children's Healthcare of Atlanta, 1400 Tullie Road NE, Atlanta, GA 30329, USA
- ¹³ Children's Hospital Los Angeles, Neuropsychology Core of the Saban Research Institute, 4661 Sunset Blvd., Los Angeles, CA 90027, USA
- ¹⁴ Division of Pediatric Cardiology, Department of Pediatrics, University of Utah School of Medicine, 30 N 1900 E, Salt Lake City, UT 84132, USA
- ¹⁵ Division of Pediatric Cardiology, Children's Hospital Los Angeles, 4650 Sunset Blvd., Los Angeles, CA 90027, USA
- ¹⁶ Division of Pediatric Cardiology, Department of Pediatrics, Duke University School of Medicine, 7506 Hospital North, DUMC Box 3090, Durham, NC 27710, USA
- ¹⁷ Division of Pediatric Cardiology, Medical University of South Carolina, 96 Jonathan Lucas St. Ste. 601, MSC 617, Charleston, SC 29425, USA
- ¹⁸ Program for Pediatric Cardiomyopathy, Heart Failure, and Transplantation, New York-Presbyterian Morgan Stanley Children's Hospital, 3959 Broadway MSCH North, 2nd Floor, New York, NY 10032, USA
- ¹⁹ Fetal Heart Program, Cincinnati Children's, 3333 Burnet Avenue, Cincinnati, OH 45229, USA
- ²⁰ Division of Pediatric Cardiology, Children's Healthcare of Atlanta, 1400 Tullie Rd NE Suite 630, Atlanta, GA 30329, USA
- ²¹ Section of Pediatric Critical Care, Department of Pediatrics, Comer Children's Hospital, University of Chicago Medicine, 5721 S. Maryland Avenue, Chicago, IL 60637, USA
- ²² Department of Pediatrics, Medical College of Wisconsin Section of Pediatric Critical Care, 9000 W. Wisconsin Avenue MS 681, Milwaukee, WI 53226, USA
- ²³ Heart Failure and Transplant Program, Children's Hospital of Philadelphia, 3401 Civic Center Blvd., Philadelphia, PA 19104, USA
- ²⁴ Department of Pediatrics, Division of Cardiology, C.S. Mott Children's Hospital, 1540 E Hospital Dr #4204, Ann Arbor, MI 48109, USA



Citation: Schmithorst, V.; Ceschin, R.; Lee, V.; Wallace, J.; Sahel, A.; Chenevert, T.L.; Parmar, H.; Berman, J.I.; Vossough, A.; Qiu, D.; et al. Single Ventricle Reconstruction III: Brain Connectome and Neurodevelopmental Outcomes: Design, Recruitment, and Technical Challenges of a Multicenter, Observational Neuroimaging Study. *Diagnostics* **2023**, *13*, 1604. <https://doi.org/10.3390/diagnostics13091604>

Academic Editors: Kim M. Cecil and Stefan Bluml

Received: 5 April 2023
Revised: 25 April 2023
Accepted: 27 April 2023
Published: 30 April 2023



Copyright: © 2023 by the authors. Licensee MDPI, Basel, Switzerland. This article is an open access article distributed under the terms and conditions of the Creative Commons Attribution (CC BY) license (<https://creativecommons.org/licenses/by/4.0/>).

* Correspondence: panigrahya@upmc.edu; Tel.: +1-412-692-5510; Fax: +1-412-692-6929

Abstract: Patients with hypoplastic left heart syndrome who have been palliated with the Fontan procedure are at risk for adverse neurodevelopmental outcomes, lower quality of life, and reduced employability. We describe the methods (including quality assurance and quality control protocols) and challenges of a multi-center observational ancillary study, SVRIII (Single Ventricle Reconstruction Trial) Brain Connectome. Our original goal was to obtain advanced neuroimaging (Diffusion Tensor Imaging and Resting-BOLD) in 140 SVR III participants and 100 healthy controls for brain connectome analyses. Linear regression and mediation statistical methods will be used to analyze associations of brain connectome measures with neurocognitive measures and clinical risk factors. Initial recruitment challenges occurred that were related to difficulties with: (1) coordinating brain MRI for participants already undergoing extensive testing in the parent study, and (2) recruiting healthy control subjects. The COVID-19 pandemic negatively affected enrollment late in the study. Enrollment challenges were addressed by: (1) adding additional study sites, (2) increasing the frequency of meetings with site coordinators, and (3) developing additional healthy control recruitment strategies, including using research registries and advertising the study to community-based groups. Technical challenges that emerged early in the study were related to the acquisition, harmonization, and transfer of neuroimages. These hurdles were successfully overcome with protocol modifications and frequent site visits that involved human and synthetic phantoms.

Keywords: hypoplastic left heart syndrome; brain connectome; harmonization; multi-center neuroimaging; phantoms

1. Introduction

In the current era of cardiothoracic surgery, children with hypoplastic left heart syndrome (HLHS) are more likely to survive into adulthood than in previous eras. Improved survival has unmasked significant morbidity including neurodevelopmental and psychosocial impairments that have been shown to affect school performance, employment, and quality of life [1–10]. The etiology of neurodevelopmental impairment in single ventricle patients is multifactorial and includes reduced in utero blood flow, low birth weight, presence of genetic abnormalities, prolonged cyanosis, congestive heart failure, unstable hemodynamics during the perioperative period, and the need for multiple cardiac catheterization and serial operations with prolonged hospital stays [11–16]. Modeling of neurodevelopmental outcomes in single ventricle patients that incorporates these risk factors is only modestly predictive, explaining less than one third of the variation in outcomes [17,18]. Many reports have documented widespread brain abnormalities in individuals with single ventricle throughout their lifespan, suggesting brain topology may be a potent biomarker that can predict neurodevelopmental outcome [19–28]. However, few of these neuroimaging studies have linked brain MRI findings to neurodevelopmental outcomes [24,29] or to specific clinical factors, suggesting that new approaches for evaluating the brain in patients with complex CHD are needed.

The Single Ventricle Reconstruction (SVR) III Brain Connectome study aims to bridge this gap by taking full advantage of methodological and conceptual developments showing that the human brain is intrinsically organized into large-scale, coherent brain networks (topology) that can be understood using methods such as graph theory analysis [24,30–36]. This study utilizes a global “systems-level” approach involving characterization of brain network connectivity, or brain “connectome,” in SVR III study participants [30–33]. We previously applied brain connectivity graph analysis to adolescent participants of the landmark Boston Circulatory Arrest Study (BCAS), in which neonates with dextro-transposition of the great arteries (d-TGA) were randomized to two different perfusion strategies and followed closely with serial neurodevelopmental assessments until the adolescent period [37–40]. Our findings in the BCAS cohort demonstrated that brain connectivity/graph

analysis could distinguish multi-domain cognitive deficits from specific neurobehavioral phenotypes (e.g., ADHD), and also delineate specific relationships between neonatal perioperative variables and long-term neurocognitive outcomes in adolescents with d-TGA. Other recent studies have described anomalous diffusion tensor-based connectome in CHD neonates and infants in both preoperative and postoperative periods, finding distinct patterns of structural network topology alterations [41–45]. Recent literature also suggests that genetic factors might impact the structural connectome in CHD [43]. However, there remains a dearth of brain connectomic analyses in pediatric/adolescent CHD. Therefore, we anticipate that applying brain connectivity analysis to the SVR cohort will lead to new insights into understanding the relationships between clinical risk factors and cognitive/behavioral outcomes in children with HLHS and other related single right ventricle cardiac malformations. Based on our prior brain DTI connectome in TGA patients, we hypothesized that the SVR III patients would have reduced global efficiency, increased modularity, and increased small-worldness compared to controls [46].

Here, we present the study design for the NHLBI-funded Pediatric Heart Network (PHN) SVR III Brain Connectome study, which has finished enrollment and data collection. We discuss our experience with recruitment and technical challenges and our implementation of solutions that resulted in meeting our adjusted enrollment goals approximately one year after the completion of the parent study (during the COVID-19 pandemic) [47]. We also present our plans for final data processing and final statistical analysis.

2. Materials and Methods

2.1. Study Design and Funding

The NHLBI-funded PHN SVR III study, “Long-term Outcomes of Children with HLHS and the Impact of Norwood Shunt Type,” is a prospective follow-up study of an existing cohort of children with HLHS and other single RV anomalies who were enrolled as newborns in a randomized clinical trial of the Norwood procedure with a modified Blalock-Taussig-Thomas shunt (MBTTS) versus a right ventricular-to-pulmonary artery shunt (RVPAS). The SVR III study was designed to determine whether the shunt assignment at the time of the Norwood procedure is associated with cardiac function, transplant-free survival, exercise function, and neurodevelopmental outcomes at ages 10 to 12 years. Transplant-free survivors of the original SVR trial were invited to participate in the multidisciplinary evaluation, including performance of a cardiac MRI, echocardiogram, exercise testing, and neurocognitive evaluations (Table 1). In the ancillary Brain Connectome Study to the SVR III study, selected SVR sites added a brain imaging component to the standard follow-up testing in the parent SVR III study. Specifically, we compared findings in SVR participants using brain imaging in concert with a complete neurodevelopmental battery and clinical information collected through the SVR III study to findings in healthy controls.

Table 1. SVR III Study procedures: schematic showing the parent SVR III study procedures that were prioritized before ancillary study procedures (brain MRI).

	8AM	9AM	10AM	11AM	12PM	1PM	2PM	3PM	4PM
Day 1	Ramped Cycle Exercise Test			Cardiac MRI		Lunch	Echo		
Day 2	Neurodevelopmental Testing			Lunch	ND Testing (Cont’d)		Brain MRI		

We will pursue the mapping of brain connectivity using two state-of-the-art neuroimaging techniques: (1) mapping structural connectivity using diffusion tensor imaging (DTI) to assess white matter tracts; [34,38,48–50] and (2) mapping functional connectivity using large-amplitude spontaneous low-frequency (<0.1 Hz) fluctuations in the functional MRI or “resting” BOLD signal that is temporally correlated across functionally related regions of the brain [51–55]. These data will be analyzed using cutting-edge quantitative complex network construction with graph theory to construct a brain connectome to characterize brain network topology [30–33]. By combining these innovative techniques within

the setting of the PHN SVR long-term follow-up study (SVR III), our specific aims are: 1. to characterize the global brain network topology of the SVR III cohort compare to healthy referents; 2. to determine which neurocognitive and behavioral outcomes are predicted by global brain network topology; 3. to determine which patient factors (e.g., birth weight, gestational age, and maternal education) and medical factors (e.g., intraoperative techniques during the Norwood procedure, hemodynamic complications, types and a number of interventions, and measures of global morbidity) predict global brain network topology; and 4. to precisely characterize inter-relationships between global brain network topology, patient/medical factors, and adverse neurocognitive/behavioral outcomes and quality of life.

2.2. Screening, Consent, and Entry Criteria for Parent and Ancillary Study

The SVR III study subjects were initially eligible to participate in the Brain Connectome Study at 10 to 12 years of age. Over the course of the study period, the participation window was extended to age 12.5 years, and then, ultimately, to any age reached by a participant by the close of the study in September 2020, when the oldest SVR subject was 15 years of age. The Principal Investigator at each site, their designees, and the study coordinator were responsible for participant recruitment into the ancillary study. All SVR III subjects were contacted to assess vital status. The transplant-free survivors were approached to participate in the ancillary study at in-person assessment SVR III study visits. SVR Trial subjects who underwent cardiac transplantation or biventricular conversion were excluded. The inclusion criteria were transplant-free survivors of the SVR cohort. The exclusion criteria included: MRI contraindication (i.e., claustrophobia, braces, metal screen failure).

2.3. Sites, Participants and Imaging Acquisition Protocol

PHN sites with more than ten eligible SVR III participants were initially invited for site participation in the SVR III Brain Connectome study. In addition, each site was asked to complete a detailed MRI questionnaire related to 3T neuro scanner capabilities (including vendor type, ability to run resting BOLD, 45 direction isotropic DTI, and research capacity for running a special customized multiband DTI-256 direction). We also queried for availability and interest of neuro-based personnel, including a neuroradiologist, MR physicist, and MR technologists' presence and capability. We developed an imaging protocol in which at least one of the connectome sequences at 3T (42-direction DTI) could be performed at all potential PHN recruiting sites. We also developed the rest of the neuroimaging protocol to facilitate the acquisition of multi-band multi-shell HARDI diffusion imaging and multiband resting state, in addition to volumetric T2 and T1 3D imaging, which was in alignment with the Adolescent Brain Cognitive Development (ABCD) study [56], accounting for the variability of the gradient strengths of the scanner (Supplementary Table S1).

2.4. Multicenter MRI Quality Assurance and Quality Control (QA/QC)

For this study, we used Siemens and Phillips 3T MRI systems. We conducted a methodological PHN inter-site reliability study to assure that the studies performed on these systems could be compared [57,58]. As proof of concept, we analyzed human multimodal data (resting BOLD, DTI, and MR spectroscopy) from five PHN sites with standardized protocols for Siemens and Philips units on a small sample of control subjects who were age-matched to the SVR subjects ($n = 10$). The temporal signal-to-noise ratio (tSNR) of the Siemens and Philips resting BOLD data was comparable (Siemens: average SNR = 169; Philips: average tSNR = 161; 4 mm × 4 mm × 4 mm voxel size). We also found that the DTI data had a similar distribution of FA values for the two vendors. In addition, we noted that the quality of spectra showed no significant differences in line width, SNR, or reliability of measurements, suggesting the feasibility of high-quality multi-site MRS data. These data suggested that reliable neuroimaging data could be obtained across the PHN sites, and these metrics were integrated into our QA/QC protocol.

Proper QA/QC procedures are complex multi-step processes that involve both phantom and subject data. We adapted a QA procedure [59] used by multiple NIH-funded multicenter studies including the Human Brain Connectome, TRACK-TBI, Pediatric Brain Tumor Consortium (PBTC), and the ABCD study [60–68]. For our prospective QA plan, each site scanned at least two phantoms (ACR-anatomic and f-BIRN-functional) for QA purposes on months that a subject was scanned (approximately once/month/site). While our initial plan was to obtain diffusion QA data using the NIST phantom, we utilized a synthetic HARDI phantom, given the single band and multiple band/multi-shell protocol that was incorporated into the study [69–71]. For the DTI phantom and human studies, we evaluated multiple values: (1) SNR at the center and periphery of the phantom; (2) comparison of image distortion in phase-encoding direction between EPI and spin echo image; and (3) comparison of image distortion between nonzero b-value DWI and b = 0 image caused by gradient encoding directions. From this, we corrected for image distortion in EPI readout caused by B_0 inhomogeneity, distortion caused by eddy currents induced by diffusion-encoding gradients, uniformity of the b-value along different diffusion-encoding directions, and correct calibration for accurate diffusivity measurements. For resting state data and the fBIRN phantom, we used Weisskoff plots and guidelines of the fBIRN research group, including average tSNR [72–76]. For anatomic quality (T1/T2 weighted), we incorporated metrics [59] including geometry accuracy, high contrast spatial resolution, the accuracy of slice thickness and position, image intensity homogeneity, and low-contrast object detectability. The QA/QC procedure was used to establish compatibility of data from different sites and long-term reproducibility of the results at each location.

2.5. Data Collection, Data Transfer and Participant Data Acceptance

Data were acquired from multiple sites from two different scanner platforms, which are likely to produce different sample means as well as different variances [56]. Imaging data transfer from the study sites was performed through a secure virtual private network (VPN) login into our network at Pediatric Imaging Research Center at Children’s Hospital of Pittsburgh, contained within the University of Pittsburgh secure firewall. File transfer used an encrypted secured file transfer protocol (SFTP), with user authentication ensuring only approved users can connect to our portal. The upload portal was developed at the University of Pittsburgh, built on the XNAT framework. XNAT is an open-source informatics platform developed at Washington University specifically for high throughput management and sharing imaging data, including connectivity data [65,77–79]. This platform is highly extensible and contains a robust network security foundation. The portal has study-specific user management, which allows the site-specific users to input de-identified participant and protocol information and images in native DICOM format, to enforce uniformity across sites. Furthermore, the XNAT framework provides for the incorporation of advanced processing pipelines, which allows each study site to perform data integrity checks and quality assurance before sharing the data. Long-term data storage was provided by servers at the University of Pittsburgh running a dedicated study-specific PostgreSQL database and built-in parity against data loss. The PHN clinical data from the SVR studies in the form of SAS datasets (export files) were transferred from the PHN Data Coordinating Center for analysis with the imaging findings using a secure FTP site.

2.6. Measures of Neurodevelopmental and Psychosocial Functioning

Standardized psychological assessments were performed by a psychologist and/or a supervised psychometrician at each site (Table 2). These measures were obtained in the SVR participants as part of the parent study [47] (Figure 1 and were explicitly included in our protocol for assessing the healthy controls. Comprehensive assessment of all domains of function including intellectual, language, visual spatial/nonverbal, learning/memory, fine motor, attention/executive, and social skills (Table 2). Caregivers completed standardized parent report measures for attention/executive, social-emotional, behavior, adaptive, and quality of life (Table 2). Our study includes quality of life questionnaires and Behavior

Rating Inventory of Executive Functioning (BRIEF), which provides parent reporting of the child's experience in everyday life activities as potential outcome measures (Table 2). The testing required approximately five hours. Breaks were provided for snacks/lunch as appropriate for the participant. Evaluations occurred at least six weeks after any hospitalization. The psychologist or psychometrician at each site was blinded to the shunt type at the time of the Norwood procedure.

Table 2. Neurocognitive Battery for SVR III Subject and Healthy Controls.

Domain	Instruments and Subtests	Completion Time-Child	Completion Time-Respondent
Intelligence	Wechsler Intelligence Scale for Children-V (WISC-V; original test kit) Block design Similarities Matrix reasoning Digit span forward Backward Sequencing Coding Vocabulary Figure weights Visual puzzles Picture span Symbol search	65–80 min	
Math	Wechsler Individual Achievement Tests III (WIAT-III) Math problem solving Numerical operations	30 min	
Reading	Wechsler Individual Achievement Tests III (WIAT-III) Word reading Reading comprehension Pseudoword decoding	32 min	
Language	NEPSY-II Comprehension of instructions Oromotor sequence	13 min	
Executive Function and Attention	Delis-Kaplan Executive Function System (DKEFS) Tower Trail making (all 5 Trials) Verbal fluency (Letter, Category, Switching) Behavior Rating Inventory of Executive Functioning (BRIEF) Parent and teacher report Conners' III ADHD Index Parent and teacher report	35 min	15 min 8 min
Visual and Perceptual Skills	Beery Developmental Test of Visual-Motor Integration (VMI-6) Beery VMI Visual perception	8 min	
Fine Motor	Lafayette Grooved Pegboard (use administration instructions from manual record raw time in seconds)	5 min	
Memory	Wide Range Assessment of Memory and Learning (WRAML-2) Story memory, Story memory recall, Story recognition; Design memory, Design recognition; Verbal learning, Verbal Learning recall, Verbal learning recognition; Picture memory, Picture memory recognition; Finger windows; Number letter; Verbal working memory; Symbolic working memory; Sentence memory	11 min	7 min
Social Skills	NEPSY-II Theory of Mind and Affect Recognition Autism Spectrum Rating Scale (ASRS) Parent report		
Behavior	Behavioral Assessment System for Children – Second Edition (BASC-2) Parent and teacher report		20 min
Quality of Life	PedsQL Generic and Cardiac Modules Parent and Child reports		15 min
Adaptive Function	Adaptive Behavior Assessment System—Third Edition (ABAS-3) Parent report		20 min
Total Time Required		199–214 min	85 min

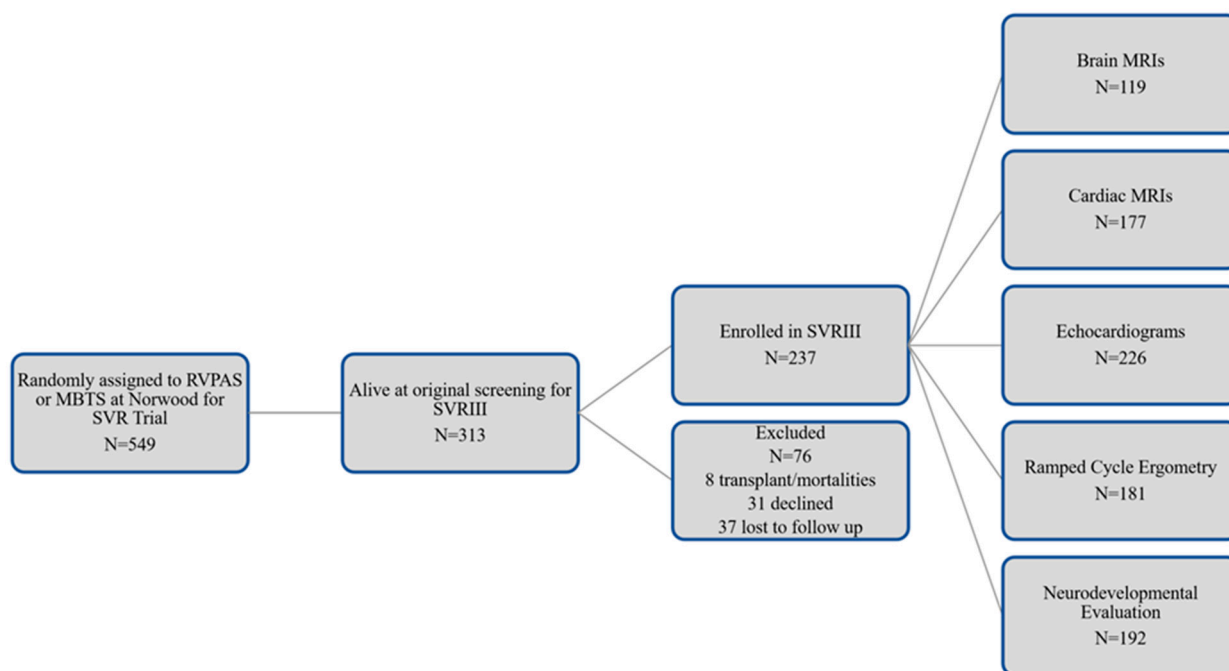


Figure 1. Original SVR Trial recruitment and SVRIII parent study enrollment.

2.7. Planned Imaging Post-Processing

Standard 45 direction-DTI, Resting BOLD data, and MB-DTI (Figure 2) will be analyzed separately for the generation of graph data.

DTI Pre-processing. All images will be corrected for motion, eddy current, and slice dropout artifacts using standard routines in FSL (FMRIB, Oxford UK). DTI data will be segmented into 90 cortical regions by applying the Brain Suite Custom Atlas [80–87] to produce cortical surface meshes and tissue classification maps.

Standard DTI. DTI metrics—including fractional anisotropy (FA), signal intensity without diffusion weighting (S0), and direction of the principal eigenvector—will be computed for each voxel. Deterministic tractography will be performed using in-house software written in Interactive Data Language (IDL) (<http://www.itervis.com>, Boulder, CO, USA; accessed 22 June 2022). Streamlines will be computed from each white matter voxel (determined as all voxels with $FA > 0.25$) in both directions. Stopping thresholds for the tractography will be turning angle > 45 degrees or $FA < 0.25$.

MB-DTI. For the MB-DTI data, due to the large number of directions, the orientation distribution function (ODF) will be computed according to routines in DSI Studio [88–90]. Tractography will be performed according to routines in DSI Studio. The ODF allows for the detection of crossing fiber tracts within a voxel and thus allows a more accurate reconstruction of fiber tracts than is possible with standard DTI. A more accurate metric of anisotropy generalized fractional anisotropy (GFA) will also be computed. Streamlines will be computed from each white matter voxel ($GFA > 0.25$) and stopping thresholds will be turning angle > 45 degrees or $GFA < 0.25$.

Graph Construction DTI. Weighted graphs (estimate of connection strength between two regions) will be computed based on: (1) the total number of streamlines beginning and ending at two regions; and (2) the average FA or GFA value of all streamlines beginning and ending at two regions.

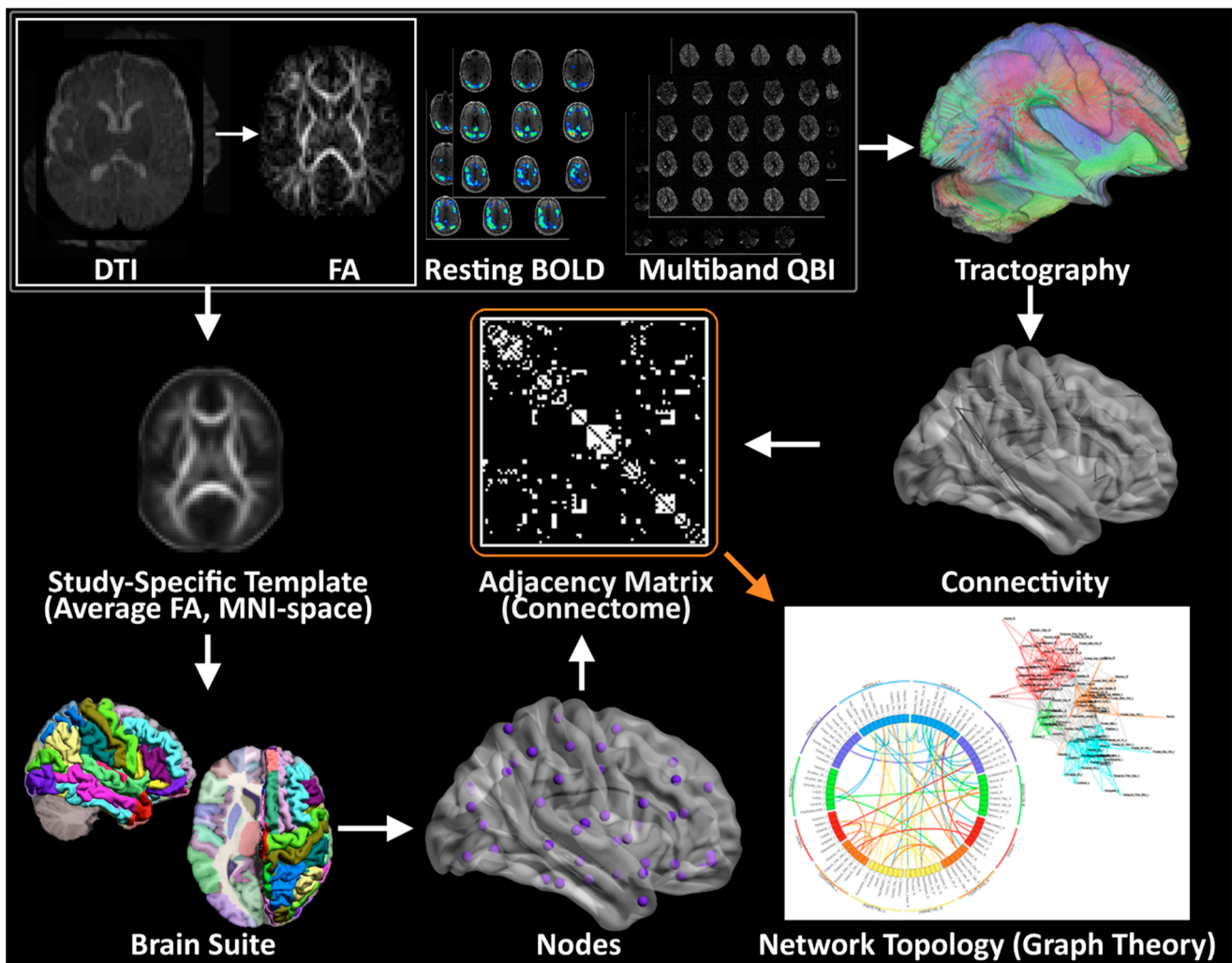


Figure 2. Methodology for Structural and Functional Network Topology Analysis. A flow diagram for the construction of WM structural and functional networks from DTI, Resting BOLD and multi-band DTI including registration, segmentation, generation of WM fiber tracts using deterministic tractography, generation of adjacency matrix and nodes, and visualization of connectivity with spring-board and circle diagrams.

Resting BOLD. The Resting BOLD data will be processed through a robust motion detection and correction pipeline described by Powers et al., [91,92] which involves volume censoring according to motion and intensity metrics, low-pass filtering, and regressing out of nuisance variables including motion parameters and global signal. The Resting BOLD data will also be parcellated using the Brain Suite atlas into 90 cortical regions. Correlation matrices will be constructed with each matrix element equal to the cross-correlation of the fMRI time series averaged in each of two regions.

Graph construction (Resting BOLD). Binary unweighted graphs will be computed based on thresholding the correlation matrices at various values of cost ranging from 0.05 to 0.45 [93].

Graph analysis. Graph metrics (global efficiency, modularity, and transitivity) [94] will be computed via the C++ modules available from the Brain Connectivity Toolbox (BCT; Indiana University) (For further details, see the BCT documentation at <https://sites.google.com/site/bctnet/> and ref. [95]). Small-worldness, another graph metric, will be computed using routines in IDL. For Resting BOLD (Blood Oxygen Level Dependent), values of the graph theory metrics will be averaged over all values of cost [96]. At the nodal level, participation coefficient and clustering coefficient will be computed using the BCT.

A spring load diagram and circle connectivity diagram will be used for visualization of relationships [97,98].

2.8. Planned Brain Connectome Outcome Measures

Primary outcome measure will include global graph measures derived from the 42-direction DTI data including global efficiency (primary) with modularity, transitivity, and small-worldness measured secondarily. Additionally, sub-network (anatomically defined) and nodal level (degree, participation coefficient, nodal efficiency, clustering coefficient) will be measured secondarily depending on the global metrics previously delineated. A similar approach will be applied to other imaging modalities collected (Resting BOLD, HARDI, etc.).

2.9. Planned Statistical Analysis

Using a standard generalized linear model, we will compare global metrics (efficiency, transitivity, modularity, and small-worldness) and sub-network/nodal metrics (clustering coefficient and participation coefficient) between the SVR III and control cases.

Analysis of indirect effects: To precisely determine the effect of single ventricle diagnosis on network topology (and ultimately on neurocognitive outcome), we will perform a statistical mediation analysis, as we have previously defined [99]. In these analyses, single ventricle diagnosis status (verses control) will be the independent variable, neurocognitive outcome will be the dependent variable, and the graph metrics will be mediating variables (with the same covariates as the standard generalized linear model above). Bootstrapping (25,000 iterations, resampling with replacement) will be used to test for statistical significance, as the indirect effect (which is the product of two regression parameters) has a well-known non-normal distribution. Bias-corrected and accelerated confidence intervals [100], shown to provide accurate control with optimal power for mediation analyses [101], will be computed. Since many mediating variables will be tested, the false discovery rate (FDR) method [102] will be used to control for false positives at $q < 0.05$. Additionally, to assess the possible effects of perioperative variables, further analyses will be conducted on the cohort of SVR participants with perioperative variables, the independent variable, neurocognitive outcome of the dependent variable, and graph metrics of the mediating variables. These analyses will be performed on a global basis and only at a sub-network/nodal level as a post hoc analysis. Correlation of structure and function will be estimated with: (1) visual correlations of nodal mapping; and (2) using AAL template anatomically-defined seed region processing of resting state fMRI and DTI data.

Covariate Measures (Independent Risk Factors): The unique nature of this large inception SVR III cohort presents the opportunity to examine the association between the clinical events that commonly occur in this population in relation to brain connectivity and neurodevelopment, as we did for the BCAS trial. Covariates that are available from the SVR trial and SVR follow-up studies (SVR II, III) include extensive pre-operative, peri-operative and annual follow-up measurements. We will prioritize those variables that are known to be associated with poor neurodevelopmental outcomes (Table 3).

Power analysis: We calculated the required sample size for 80% power and the two-sided $\alpha = 0.05$ to detect effect sizes estimated from the graph theory data on DTI in the BCAS (preliminary data) in relation to the global metrics for aims 1–3 using G*Power 3.1.3. Effect sizes f^2 were computed as (variance explained by effect)/(error variance), converted to effect size f for aim 1 as the desired input in G*Power 3.1.3. Effect sizes of $f^2 < 0.15$ ($f < 0.39$) are considered to be small effects. Aim 1: The effect sizes for differences between SVR participants and controls are: (a) global efficiency: effect size $f = 0.29$, requires a sample size of 97 subjects total for 0.8 power; (b) modularity: effect size $f^2 = 0.15$ requires a sample size of 54 subjects total for 0.8 power; and (c) small worldness: an effect size of $f = 0.34$ requires a sample size of 69 subjects for 0.8 power. Aim 2: The effect size for the correlation between full-scale IQ and global efficiency (combined SVR/control group) is estimated to be $f^2 = 0.093$, requiring a sample size of 87 subjects for 0.8 power.

A similar given power was detected for other domains (visual spatial, memory, executive function), which were also tested in the BCAS study. Aim 3: The effect size for the correlation between total cooling time and global efficiency in the SVR cohort is estimated to be $f^2 = 0.096$, requiring a sample size of 84 subjects for 0.8 power and $p = 0.05$. These calculations demonstrate that the required sample size to detect effect sizes similar to those observed in the BCAS with 80% power are all smaller than our initially targeted sample size of 140 SVR subjects and 100 referents. Furthermore, the study is well-powered to detect small effect sizes for our study hypotheses. From this power analysis, we determined that a sample size of at least 100 SVR subjects with analyzable MRI data would be ideal. Given that we expected a certain portion of SVR participants to fail the imaging procedures (based on non-compliance and too much motion artifact), we decided to initially target approximately 140 total SVR participants, expecting 1/3 of data points to be unanalyzable. We also initially targeted 100 age-matched controls to be recruited from the same sites. Therefore, our initial planned targeted enrollment for the study was approximately 240 subjects (SVR + Controls).

Table 3. Examples of longitudinal clinical risk factors in the SVR Trial Dataset [47].

Pre-Stage I and Demographics	Stage I, II, III Hospitalization	Medication Use	Procedural History Data
<ul style="list-style-type: none"> • prenatal diagnosis • genetic syndrome • birth weight • gestational age • intubation • socioeconomic status • maternal education 	<ul style="list-style-type: none"> • mechanical ventilation time • cardiopulmonary bypass and deep hypothermic circulatory arrest/regional cerebral perfusion times • ICU/hospital length of stay • delayed sternal closure • use of extracorporeal membrane oxygenation (ECMO) • unplanned surgical/catheter interventions 	<ul style="list-style-type: none"> • treatment with heart failure medications (angiotensin-converting enzyme inhibitors) • angiotensin receptor blockers, beta blockers • treatment for pulmonary hypertension • use of anticoagulation 	<ul style="list-style-type: none"> • unanticipated interventions (catheterization or surgery, such as pacemaker implantation, stent implantation, Fontan revision) • lack of Fontan completion

2.10. Initial Recruitment Challenges

In this ancillary study of the longitudinal SVRIII parent study, we aimed to add a brain imaging component in addition to the parent’s study multidisciplinary evaluation including the performance of a cardiac MRI study, echocardiogram, exercise testing, and neurocognitive evaluations over two full days (Table 1). To avoid interference with the parent study, we performed the brain MRI component after the measures required for the parent study. However, while most participants completed the full program for the parent study, some participants and parents deemed the extra allotted time for the MRI too taxing, especially after the neurocognitive assessment. While incentives and extra travel accommodations were available to reschedule the brain MRI, some participants were lost to this ancillary study who were enrolled in the main SVR study.

To counteract participant fatigue and avoid losing participants, we devised a strong coordinator-driven explanation of the study, and direct benefits to the participants and indirect benefits to the community in general to increase interest. We also increased the number of meetings with direct key study personnel (study investigators, e.g., doctors, coordinators, MRI specialists) to enhance successful participant recruitment for this ancillary study. We devised a bi-monthly call between coordinators of all sites to discuss challenges and help each other identify various successful recruitment strategies. These twice-monthly

multi-site coordinator calls were extremely well-attended and allowed communication between sites regarding recruitment difficulties, addressing MRI safety and screening issues, and reviewing case report forms and protocol revisions. Strategies to recruit healthy controls were expanded at multiple sites to include the use of clinical translational research registries, pediatric clinics seeing healthy patients, and community sites (schools, churches, and special neighborhoods). Of note, ADHD is more prevalent in the HLHS population, and our neuroimaging protocol was designed to maximize data acquisition but minimize scanner time. We also increased the number of enrolling sites to assist with the enrollment of both SVR and control subjects.

2.11. Initial Technical Challenges

Some of the initial technical challenges of the study were related to imaging acquisition, imaging harmonization, and data transfer/storage. With regard to image acquisition, there were challenges to the acquisition of multi-band (MB) BOLD and HARDI scans (Figure 3). Many of the errors were operator errors. Both MB scans require a reference scan to be acquired prior to running the main body of sequences for purposes of reconstruction. Hence, running the main body of sequences without first running the reference scan was a common mistake. A related mistake was copying scan parameters from BOLD images or using the BOLD reference image for HARDI sequences, which have different image and slice resolutions, resulting in lower resolution HARDI images and an unusable data set. Another common mistake was prescribing an inadequately-sized shim box, resulting in distorted HARDI images. Less frequent but still encountered was the failure to turn on coil elements, leading to images with low SNR. Lastly, in a few cases, fat saturation bands, used to estimate multiband coverage by some sites, were left on, leading to images with a swath of HARDI image slices with suppressed signal. These errors were documented in a technical manual and information was disseminated to all sites to prevent these errors from recurring. In addition, frequent site visits were conducted to provide education about these issues.

With regard to imaging harmonization, given the anticipated scanner variance from using two different vendor scanners, QA/QC procedures include a complex multi-step harmonization process that involves: (1) development and surveillance of a standardized neuroimaging protocol across sites; (2) prospective ongoing synthetic and human phantom studies to provide cross-calibration across scanner; and (3) retrospective or statistical harmonization of human subject neuroimaging data, knowing that inter-scanner variation will still occur despite the implementation of (1) and (2). To address some of these issues, we increased the number of both synthetic and human phantom data (a total of five human phantoms and two synthetic phantoms scanned three times) (Figure 4). We specifically introduced the use of a HARDI phantom, given the data that were being collected in the study, knowing that diffusion imaging tends to have the greatest inter-scanner variance even after protocol matching. We currently have a database of greater than 100 synthetic and single human phantom HARDI diffusion tensor data on PHN 3T MRI scanners (Siemens/Phillips vendors). We have recently developed a new pipeline that incorporates both synthetic phantom and human individual subject-specific template/tract generation via a semi-automated approach. This dataset will allow for future analyses that can directly estimate the effect of scanner type. For diffusion MRI, our synthetic phantom simulates various axonal configurations including varying density, fiber crossing, etc., constructed from textile “taxons” of similar diameter to actual axons. By scanning the phantom repeatedly across sites, estimates may be obtained for within-site and across-site variability, and these estimates may be incorporated into the final analysis. However, this approach is limited by the type of diffusion metrics that can be estimated using the phantom, such as voxelwise fractional anisotropy or mean diffusivity, and is unavailable if more advanced diffusion metrics (e.g., along-tract FA/MD values derived from tractography, estimates of myelin water fraction, graph analysis parameters, etc.) are desired that cannot be computed from the phantom. For these more advanced metrics, we will be able to utilize our human

phantoms, which are scanned repeatedly at each site. Again, these data will yield estimates of within- and across-site variability for each desired parameter, which can be incorporated into the final analysis.

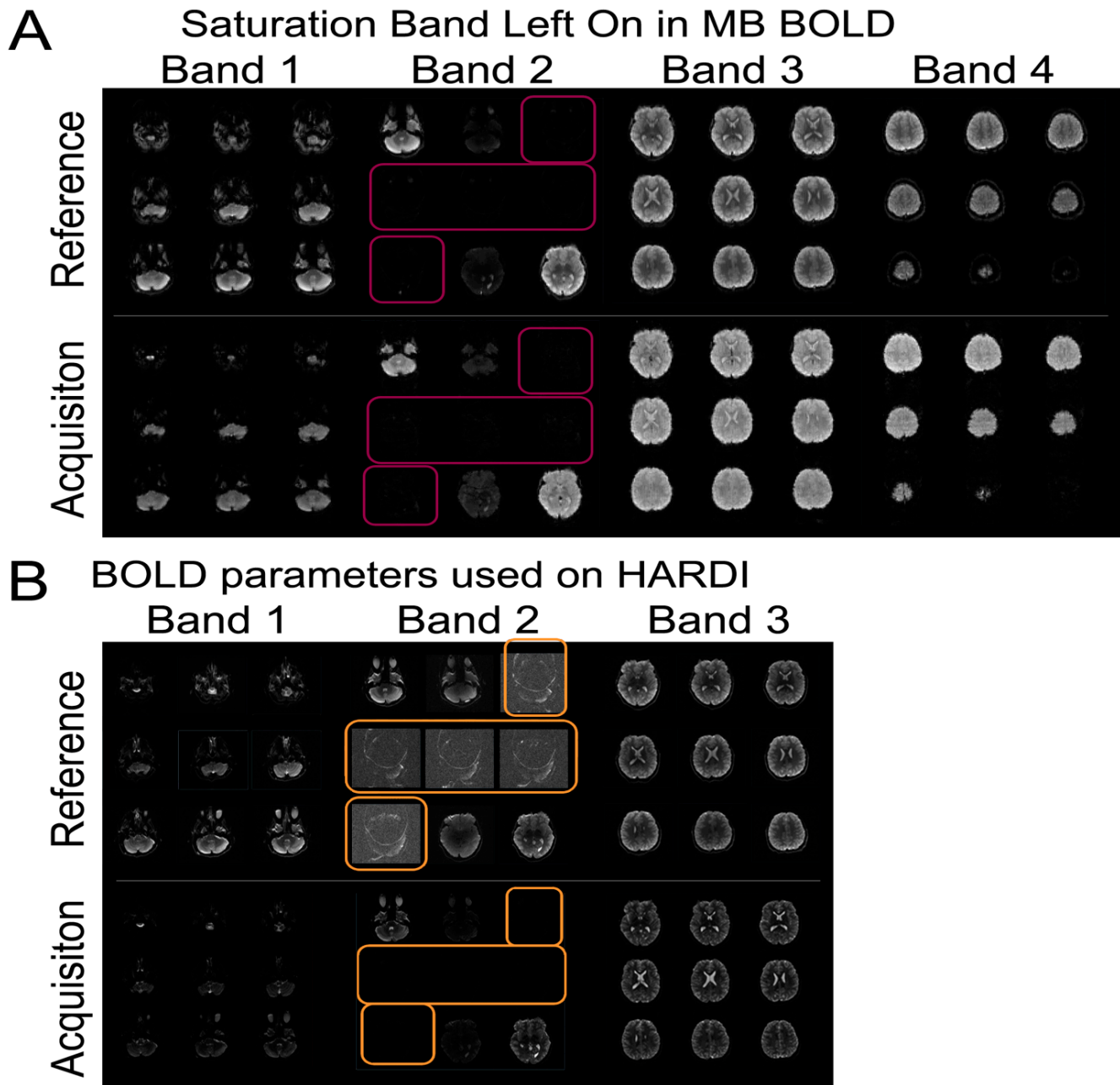


Figure 3. Multi-band reference scan error example with: (A) saturation band left on the BOLD imaging; and (B) ultimately propagated to the DTI/HARDI prescription and acquisition in error. These errors underscore the need for a technical manual, ongoing QA of data, and technological training.

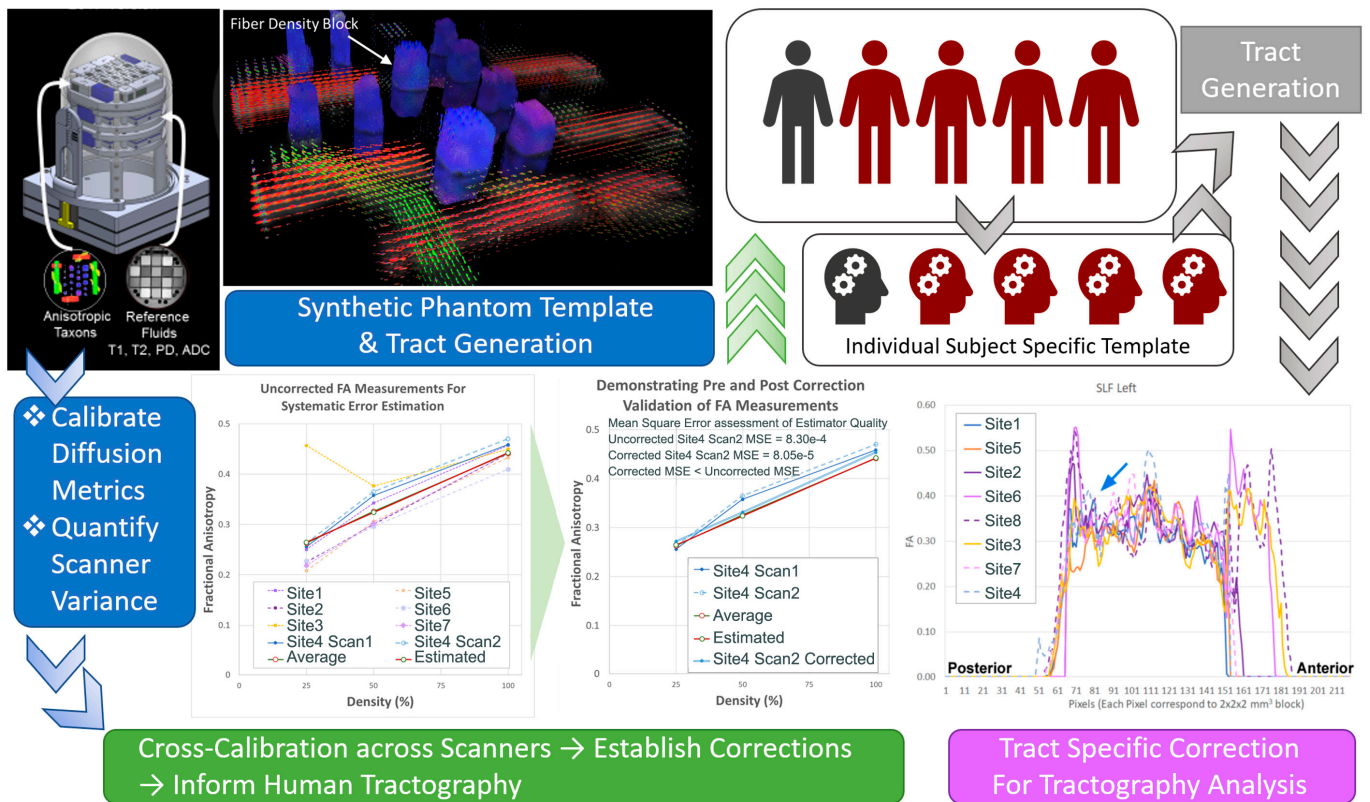


Figure 4. Harmonization Design: We used synthetic and human phantom and a semi-automated pipeline to generate tract-specific information to estimate inter-scanner variance and then applied this to the in vivo analysis. Bottom-left: FA measurements of taxon blocks from seven PHN sites. The results show a reduced variability in the calibrated FA in the corrected scan (blue double line) compared to the uncorrected scan (blue dotted line). Bottom-right: along-tract FA analysis of an individual human phantom across multiple sites. The tract shown is the left SLF showing portions of tract that are more sensitive to scanner variability (blue arrows).

With regard to image transfer, some of the sites were within secure hospital firewalls, while other sites were within pure research imaging environments. To address the variability in firewalls and ability to transfer de-identified neuroimaging data, we set up our study database using the open-source neuroimaging specific framework XNAT. We then customized a secure, externally accessible portal on our University of Pittsburgh domain with standardized forms for demographics and data entry. Our protocol provided two options for each site to upload imaging data: (A) directly to our XNAT database, accessible via the web portal; and (B) via an sFTP transfer into a local server behind our firewall. Option A was the preferred method, as images were directly archived into our database and linked to the appropriate subject data. We required sites to anonymize the studies prior to uploading (regardless of upload method), and our XNAT server performed a secondary safety-net anonymization prior to archiving in case any remaining personal health information were present in the DICOM headers. At time of development, the upload portal required a Java plugin to upload DICOM studies. Due to varying internet security measures at each site, some of the clinical sites were restricted from using a Java plugin. In these instances, if IT support was not provided to implement a white-list exception to this plugin, sites were unable to upload the images via this method. Subject forms (including consent, demographics, and behavioral testing) were still entered here, however, as no plugin was necessary. Therefore, option B was presented as an alternative to image transfer. Via option B, DICOM studies were uploaded into our local server, and our own database manager archived it in the XNAT database. This method was used solely on a need-basis, as it required an additional step for our coordinating site, and sites were required to receive

University of Pittsburgh guest accounts with two-factor authentication (2FA), which can be a technical challenge for some users. Finally, if a site was unable to use methods A or B due to technical, security, or personnel difficulties, we requested that physical copies of the anonymized images be sent via secure courier to our facility for archival by our database manager. Updates to our technical protocol and frequent site visits to troubleshoot these image transfer issues helped with developing a robust image transfer process.

2.12. Timeline and Impact of COVID-19 Pandemic

The first participant in the SVRIII Brain Connectome study was enrolled on April 6, 2016, nine months after the first study participant was enrolled in the parent SVR III study. Planned enrollment was predicted to last until approximately April 2020 (4 years). We prolonged the extension of this ancillary study after the parent study finished enrolling in September 2019 to increase study participation up until January 2022. Importantly, the COVID-19 pandemic prevented the completion of in-person evaluations, more common over the summer, between March 2020 and August 2020 at most sites (Figures 1 and 5–7). The SVRIII Brain Connectome study, which finished enrolling in January of 2022, enrolled 125 SVRIII participants (116 analyzable scans) and 93 control participants (89 analyzable scans). From our power analysis (see power analysis section), we determined that a sample size of at least 100 analyzable SVR subjects would be ideal. As such, the final enrollment number of $n = 218$ subjects did achieve our goal.

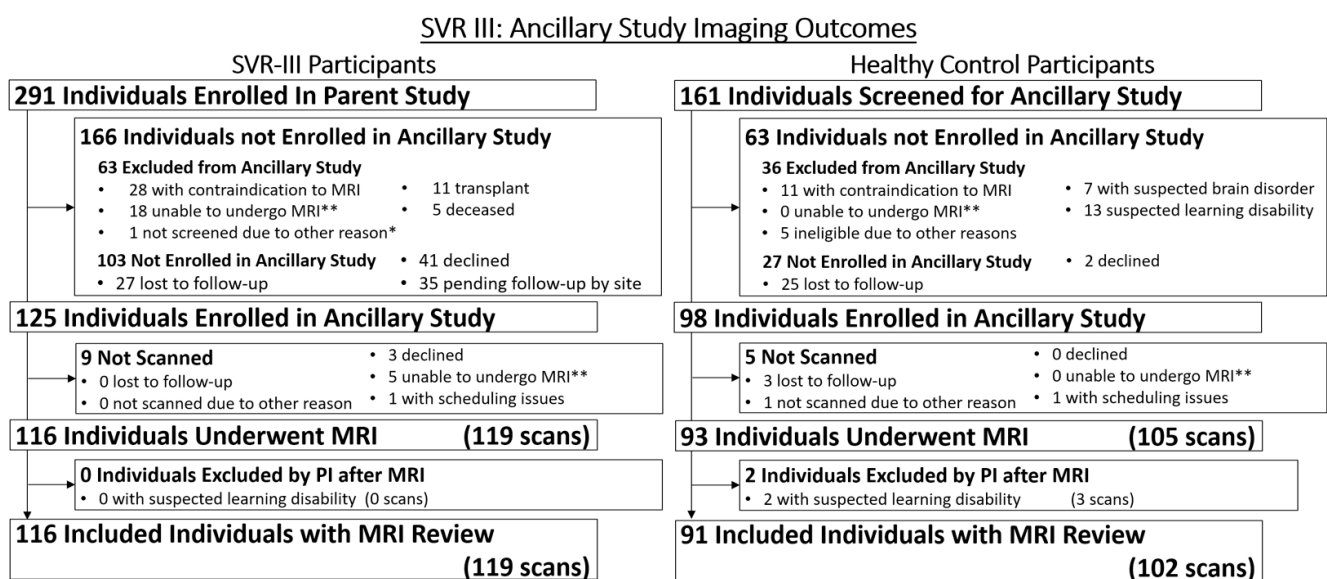


Figure 5. SVRIII Brain Connectome: Enrollment and Collections of Neuroimaging Studies for SVRIII Participants and Healthy Controls. * = only 290 SVR subjects reported from sites missing one subject from one site; ** = unable to undergo MRI due to anxiety or another issue that may be revisited.

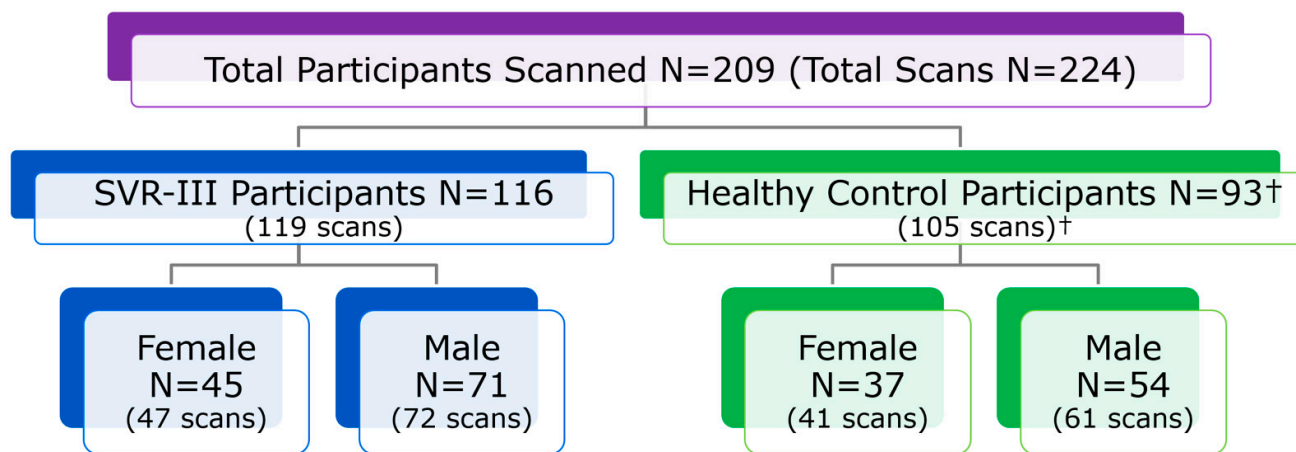


Figure 6. SVR III Brain Connectome Study: Diagnostic group and postnatal sex of enrolled participants. Notes: All included participant MRIs were reviewed. † = 2 Participants (3 scans) withdrawn after MRI.

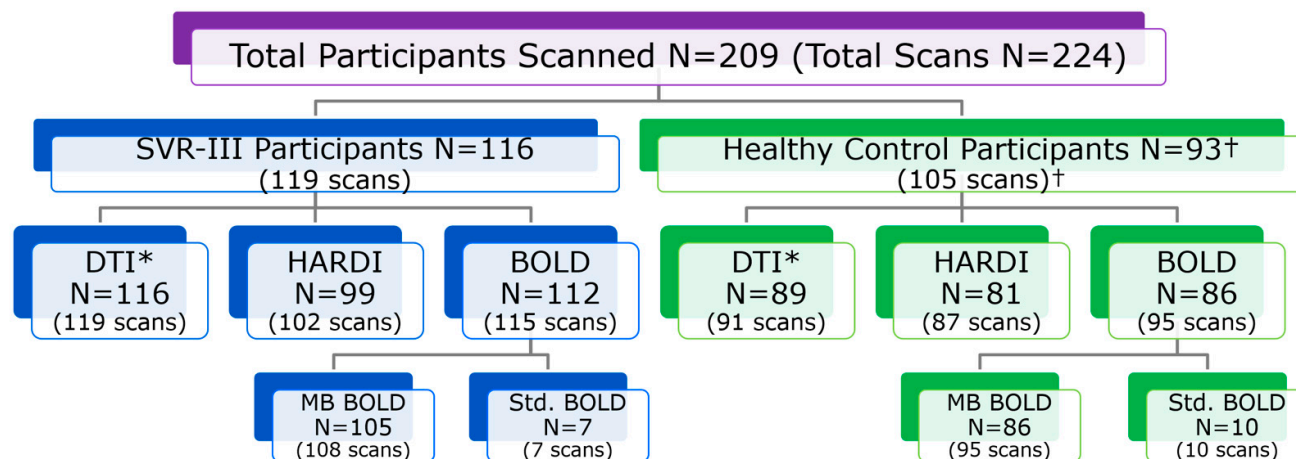


Figure 7. SVR III Brain Connectome Study: breakdown of imaging studies collected (DTI, HARDI, Resting BOLD). Notes: all included participant MRIs were reviewed. † = 2 participants (3 scans) withdrawn after MRI; * = Main Deliverable Imaging Biomarker on Study (42-direction DTI scan).

3. Results and Discussion

The SVR III Brain Connectome study will be the first to validate connectome neuroimaging biomarkers to prognosticate outcomes in early adolescent HLHS patients. It leverages a rich longitudinal dataset of HLHS patients collected as part of the parent study. The SVR III Brain Connectome study will not only help to elucidate the impact of complex CHD on brain development, but also the manner in which a developing neural architecture—connectome—gives rise to cognitive-behavioral phenotypes in the SVR III longitudinal cohort. The data generated will allow us to determine whether brain network topology can serve as a biomarker for specific behavioral and neuropsychiatric phenotypic deficits and whether peri-operative and patient factors are associated with the development of specific brain network topology. The results of these studies will provide the basis for future predictive modeling, and ultimately, targeted interventions to improve neurodevelopmental outcomes of HLHS patients.

Our study overcame several obstacles, as described in detail above. Initial lagging recruitment was successfully addressed by multiple approaches, including addition of recruiting sites and frequent multi-site coordinator calls to maintain enthusiasm and brainstorm about recruiting techniques. Technical challenges that emerged early in the study were related to neuroimaging acquisition, harmonization and transfer. We responded to

these challenges with modification of the study protocol and frequent site visits, which involved traveling human and synthetic phantoms. A specific challenge of multi-site MRI studies is harmonization of MRI data across different sites and scanner platforms. Between different MRI vendors (e.g., Philips, Siemens, GE), the same apparent MRI pulse sequence (e.g., identical parameters are entered at the console) is quite often variable in practice due to RF pulse shape, diffusion-encoding gradient (e.g., amplitudes and duration can be vendor distinct even for the identical “b-value” entered at the console), and bandwidth in slice-select direction. For the same MRI vendor but a different scanner platform (e.g., Siemens Skyra vs. Siemens Prisma), the actual pulse sequence is often different due to different hardware specifications between the two platforms (e.g., maximum gradient strength, slew rate, RF power, etc.), as the actual pulse sequence run is optimized dependent on the available hardware.

We have recently developed multiple retrospective harmonization approaches that can eventually be applied to this dataset, if needed. For example, if the number of subjects per site is adequate and the SVR III participant/control ratio is approximately equal across sites, data may be analyzed separately for each site and the final result combined afterwards, with negligible loss of statistical power. We have previously used this approach in a two-site study comparing DTI analyses (graph analysis and voxelwise) between neonates with CHD and healthy controls [45]. Data were analyzed separately to estimate the between-subject variance separately for each platform, and site-specific estimates were then combined to perform an aggregate analysis (with scanner platform incorporated as a nuisance parameter). Another retrospective neuroimaging harmonization approach is the empirical Bayes method (COMBAT). If the total sample size is sufficiently large, it is possible to estimate a (site-independent) prior distribution from the data itself. Site-specific correction factors are then able to be estimated and applied to the data. The final analysis is performed using the combined, harmonized data. We have recently successfully applied this COMBAT technique to a four-center DTI dataset of 763 neonates with congenital heart disease [103].

4. Conclusions

The SVR III Brain Connectome study leverages the PHN SVR III study, adding brain MRI and the inclusion of healthy controls to undergo neurocognitive evaluation and brain MRI to understand not only the basis of important brain-behavior phenotypes that are present in single ventricle patients, but also the modifiable and non-modifiable longitudinal risk factors that predict these relationships. Our study will provide further validation of brain connectome metrics about neurocognitive and neurobehavioral outcomes and essential clinical risk factors that are associated with poor brain health outcomes in pediatric neurodevelopmental disorders. Since this was a multi-center brain imaging study, harmonization was prioritized with initial protocol matching, use of human/synthetic phantoms and development of novel retrospective neuroimaging techniques. Through the conduct of this study, we learned about some of the challenges and solutions related to adding neuroimaging ancillary procedures to a parent study design. Analyses will elucidate not only the impact of single ventricle heart disease on brain development, but also the relationships between the human connectome and cognitive-behavioral phenotypes.

Supplementary Materials: The following supporting information can be downloaded at: <https://www.mdpi.com/article/10.3390/diagnostics13091604/s1>, Table S1: SVR III Brain Connectome Protocol: Harmonized Parameters for Siemens and Phillips 3T MRI.

Author Contributions: Conceptualization, A.P., V.S. and R.C.; Methodology, A.P., V.S. and R.C.; Software, V.S. and V.L.; Validation, A.P., V.S., R.C. and V.L.; Formal Analysis, A.P., V.S., R.C., V.L. and J.W.; Investigation, J.W.; Resources, A.P.; Data Curation, V.S., R.C. and J.W.; Writing—Original Draft Preparation, V.S., R.C., V.L., J.W., A.S., T.L.C., H.P., J.I.B., A.V., D.Q., N.K., P.E.G., B.G., P.S.L., M.M., L.A.S., D.C.B., D.I., S.O., T.A.M., J.D., K.D.H., A.M.A., M.E.R., J.C., W.T.M., N.S.G., J.W.G., C.S.G., J.W.N. and A.P.; Writing—Review & Editing, V.S., R.C., V.L., J.W., A.S., T.C., H.P., J.I.B., A.V., D.Q., N.K., P.E.G., B.G., P.S.L., M.M., L.A.S., D.C.B., D.I., S.O., T.A.M., J.D., K.D.H., A.M.A., M.E.R., J.C., W.T.M., N.S.G., J.W.G., C.S.G., J.W.N. and A.P.; Visualization, A.P. and V.S.; Supervision, A.P.; Project Administration, A.P.; Funding Acquisition, A.P. All authors have read and agreed to the published version of the manuscript.

Funding: This work was supported by grants from the National Heart, Lung, and Blood Institute (HL135680, HL135685, HL135683, HL135689, HL135691, HL135646, HL135665, HL135678, HL135682, and HL135666). AP was supported by the Department of Defense (W81XWH-16-1-0613), the National Heart, Lung and Blood Institute (R01 HL152740-1, R01 HL128818-05), National Library of Medicine (5T15LM007059-320), a Society for Pediatric Radiology Multi-Institutional Pilot Award and Additional Ventures.

Institutional Review Board Statement: IRB approval was obtained at each participating site and written consent obtained from parents prior to participation in SVRIII Brain Connectome. Additional oversight is provided by an NIH-appointed Data and Safety Monitoring Board and medical monitor. Parents and/or guardians are consented, and children assented (when possible) by the site PI or research coordinator for enrollment. University of Pittsburgh IRB CR19090078-003 approval 22 June 2022.

Informed Consent Statement: Informed consent was obtained from all subjects involved in the study.

Data Availability Statement: Data are contained within the article and the Supplementary Materials.

Acknowledgments: We acknowledge the hard work of the Pediatric Heart Network coordinators including Katherine Afton, Carolyn Dunbar-Masterson, Lisa Jean Buckley, Kathy Lupton, Michelle Otto, Regina Cole, Michelle Hamstra, Madison Rudow, Katrina Golub, Chanel Rojas, Mingfen Xu, Kalyan Chundru.

Conflicts of Interest: The authors declare no conflict of interest.

References

1. McCrindle, B.W.; Williams, R.V.; Mitchell, P.D.; Hsu, D.T.; Paridon, S.M.; Atz, A.M.; Li, J.S.; Newburger, J.W. Relationship of patient and medical characteristics to health status in children and adolescents after the Fontan procedure. *Circulation* **2006**, *113*, 1123–1129. [[CrossRef](#)] [[PubMed](#)]
2. Mahle, W.T.; Clancy, R.R.; Moss, E.M.; Gerdes, M.; Jobs, D.R.; Wernovsky, G. Neurodevelopmental outcome and lifestyle assessment in school-aged and adolescent children with hypoplastic left heart syndrome. *Pediatrics* **2000**, *105*, 1082–1089. [[CrossRef](#)] [[PubMed](#)]
3. Marelli, A.J.; Ionescu-Ittu, R.; Mackie, A.S.; Guo, L.; Dendukuri, N.; Kaouache, M. Lifetime Prevalence of Congenital Heart Disease in the General Population from 2000 to 2010. *Circulation* **2014**, *130*, 749–756. [[CrossRef](#)] [[PubMed](#)]
4. Goldberg, C.S.; Schwartz, E.M.; Brunberg, J.A.; Mosca, R.S.; Bove, E.L.; Schork, M.A.; Stetz, S.P.; Cheatham, J.P.; Kulik, T.J. Neurodevelopmental outcome of patients after the fontan operation: A comparison between children with hypoplastic left heart syndrome and other functional single ventricle lesions. *J. Pediatr.* **2000**, *137*, 646–652. [[CrossRef](#)]
5. Tabbutt, S.; Nord, A.S.; Jarvik, G.P.; Bernbaum, J.; Wernovsky, G.; Gerdes, M.; Zackai, E.; Clancy, R.R.; Nicolson, S.C.; Spray, T.L.; et al. Neurodevelopmental outcomes after staged palliation for hypoplastic left heart syndrome. *Pediatrics* **2008**, *121*, 476–483. [[CrossRef](#)]
6. Tabbutt, S.; Gaynor, J.W.; Newburger, J.W. Neurodevelopmental outcomes after congenital heart surgery and strategies for improvement. *Curr. Opin. Cardiol.* **2012**, *27*, 82–91. [[CrossRef](#)]
7. Wernovsky, G.; Newburger, J. Neurologic and developmental morbidity in children with complex congenital heart disease. *J. Pediatr.* **2003**, *142*, 6–8. [[CrossRef](#)]
8. Wernovsky, G.; Stiles, K.M.; Gauvreau, K.; Gentles, T.L.; du Plessis, A.J.; Bellinger, D.C.; Walsh, A.Z.; Burnett, J.; Jonas, R.A.; Mayer, J.E., Jr.; et al. Cognitive development after the Fontan operation. *Circulation* **2000**, *102*, 883–889. [[CrossRef](#)]
9. Mellion, K.; Uzark, K.; Cassidy, A.; Drotar, D.; Wernovsky, G.; Newburger, J.W.; Mahony, L.; Mussatto, K.; Cohen, M.; Limbers, C.; et al. Health-related quality of life outcomes in children and adolescents with congenital heart disease. *J. Pediatr.* **2014**, *164*, 781–788.e1. [[CrossRef](#)]

10. Shillingford, A.J.; Glanzman, M.M.; Ittenbach, R.F.; Clancy, R.R.; Gaynor, J.W.; Wernovsky, G. Inattention, hyperactivity, and school performance in a population of school-age children with complex congenital heart disease. *Pediatrics* **2008**, *121*, e759–e767. [[CrossRef](#)]
11. Goldberg, C.S.; Kathleen, M.; Daniel, L.; Gil, W. Neurodevelopment and quality of life for children with hypoplastic left heart syndrome: Current knowns and unknowns. *Cardiol. Young* **2011**, *21* (Suppl. S2), 88–92. [[CrossRef](#)]
12. Donofrio, M.T.; Duplessis, A.J.; Limperopoulos, C. Impact of congenital heart disease on fetal brain development and injury. *Curr. Opin. Pediatr.* **2011**, *23*, 502–511. [[CrossRef](#)]
13. Newburger, J.W.; Sleeper, L.A.; Frommelt, P.C.; Pearson, G.D.; Mahle, W.T.; Chen, S.; Dunbar-Masterson, C.; Mital, S.; Williams, I.A.; Ghanayem, N.S.; et al. Transplantation-free survival and interventions at 3 years in the single ventricle reconstruction trial. *Circulation* **2014**, *129*, 2013–2020. [[CrossRef](#)]
14. Nathan, M.; Sleeper, L.A.; Ohye, R.G.; Frommelt, P.C.; Caldarone, C.A.; Tweddell, J.S.; Lu, M.; Pearson, G.D.; Gaynor, J.W.; Pizarro, C.; et al. Technical performance score is associated with outcomes after the Norwood procedure. *J. Thorac. Cardiovasc. Surg.* **2014**, *148*, 2208–2214. [[CrossRef](#)]
15. Burch, P.T.; Gerstenberger, E.; Ravishankar, C.; Hehir, D.A.; Davies, R.R.; Colan, S.D.; Sleeper, L.A.; Newburger, J.W.; Clabby, M.L.; Williams, I.A.; et al. Longitudinal assessment of growth in hypoplastic left heart syndrome: Results from the single ventricle reconstruction trial. *J. Am. Heart Assoc.* **2014**, *3*, e000079. [[CrossRef](#)]
16. Volpe, J.J. Encephalopathy of congenital heart disease- destructive and developmental effects intertwined. *J. Pediatr.* **2014**, *164*, 962–965. [[CrossRef](#)]
17. Mahle, W.T.; Lu, M.; Ohye, R.G.; William Gaynor, J.; Goldberg, C.S.; Sleeper, L.A.; Pemberton, V.L.; Mussatto, K.A.; Williams, I.A.; Sood, E.; et al. A predictive model for neurodevelopmental outcome after the Norwood procedure. *Pediatr. Cardiol.* **2013**, *34*, 327–333. [[CrossRef](#)]
18. Goldberg, C.S.; Lu, M.; Sleeper, L.A.; Mahle, W.T.; Gaynor, J.W.; Williams, I.A.; Mussatto, K.A.; Ohye, R.G.; Graham, E.M.; Frank, D.U.; et al. Factors Associated with Neurodevelopment for Children with Single Ventricle Lesions. *J. Pediatr.* **2014**, *165*, 490–496. [[CrossRef](#)]
19. Limperopoulos, C.; Tworetzky, W.; McElhinney, D.B.; Newburger, J.W.; Brown, D.W.; Robertson, R.L., Jr.; Guizard, N.; McGrath, E.; Geva, J.; Annese, D.; et al. Brain volume and metabolism in fetuses with congenital heart disease: Evaluation with quantitative magnetic resonance imaging and spectroscopy. *Circulation* **2010**, *121*, 26–33. [[CrossRef](#)]
20. Clouchoux, C.; du Plessis, A.J.; Bouyssi-Kobar, M.; Tworetzky, W.; McElhinney, D.B.; Brown, D.W.; Gholipour, A.; Kudelski, D.; Warfield, S.K.; McCarter, R.J.; et al. Delayed cortical development in fetuses with complex congenital heart disease. *Cereb. Cortex* **2013**, *23*, 2932–2943. [[CrossRef](#)]
21. Miller, S.P.; McQuillen, P.S.; Hamrick, S.; Xu, D.; Glidden, D.V.; Charlton, N.; Karl, T.; Azakie, A.; Ferriero, D.M.; Barkovich, A.J.; et al. Abnormal brain development in newborns with congenital heart disease. *N. Engl. J. Med.* **2007**, *357*, 1928–1938. [[CrossRef](#)] [[PubMed](#)]
22. Licht, D.J.; Shera, D.M.; Clancy, R.R.; Wernovsky, G.; Montenegro, L.M.; Nicolson, S.C.; Zimmerman, R.A.; Spray, T.L.; Gaynor, J.W.; Vossough, A. Brain maturation is delayed in infants with complex congenital heart defects. *J. Thorac. Cardiovasc. Surg.* **2009**, *137*, 529–536; Discussion 536–537. [[CrossRef](#)] [[PubMed](#)]
23. Paquette, L.B.; Wisnowski, J.L.; Ceschin, R.; Pruetz, J.D.; Detterich, J.A.; Del Castillo, S.; Nagasunder, A.C.; Kim, R.; Painter, M.J.; Gilles, F.H.; et al. Abnormal cerebral microstructure in premature neonates with congenital heart disease. *AJNR Am. J. Neuroradiol.* **2013**, *34*, 2026–2033. [[CrossRef](#)] [[PubMed](#)]
24. Von Rhein, M.; Buchmann, A.; Haggmann, C.; Huber, R.; Klaver, P.; Knirsch, W.; Latal, B. Brain volumes predict neurodevelopment in adolescents after surgery for congenital heart disease. *Brain* **2014**, *137*, 268–276. [[CrossRef](#)]
25. Andropoulos, D.B.; Hunter, J.V.; Nelson, D.P.; Stayer, S.A.; Stark, A.R.; McKenzie, E.D.; Fraser, C.D., Jr. Brain immaturity is associated with brain injury before and after neonatal cardiac surgery with high-flow bypass and cerebral oxygenation monitoring. *J. Thorac. Cardiovasc. Surg.* **2010**, *139*, 543–556. [[CrossRef](#)]
26. Dent, C.L.; Spaeth, J.P.; Jones, B.V.; Schwartz, S.M.; Glauser, T.A.; Hallinan, B.; Kurth, C.D. Brain magnetic resonance imaging abnormalities after the Norwood procedure using regional cerebral perfusion. *J. Thorac. Cardiovasc. Surg.* **2005**, *130*, 1523–1530. [[CrossRef](#)]
27. Cordina, R.; Grieve, S.; Barnett, M.; Lagopoulos, J.; Malitz, N.; Celermajer, D.S. Brain volumetric, regional cortical thickness and radiographic findings in adults with cyanotic congenital heart disease. *Neuroimage Clin.* **2014**, *4*, 319–325. [[CrossRef](#)]
28. McQuillen, P.S.; Miller, S.P. Congenital heart disease and brain development. *Ann. New York Acad. Sci.* **2010**, *1184*, 68–86. [[CrossRef](#)]
29. Rollins, C.K.; Watson, C.G.; Asaro, L.A.; Wypij, D.; Vajapeyam, S.; Bellinger, D.C.; DeMaso, D.R.; Robertson, R.L., Jr.; Newburger, J.W.; Rivkin, M.J. White Matter Microstructure and Cognition in Adolescents with Congenital Heart Disease. *J. Pediatr.* **2014**, *165*, 936–944. [[CrossRef](#)]
30. Bullmore, E.; Sporns, O. Complex brain networks: Graph theoretical analysis of structural and functional systems. *Nat. Rev. Neurosci.* **2009**, *10*, 186–198. [[CrossRef](#)]
31. Bullmore, E.; Sporns, O. The economy of brain network organization. *Nat. Rev. Neurosci.* **2012**, *13*, 336–349. [[CrossRef](#)]
32. Griffa, A.; Baumann, P.S.; Thiran, J.-P.; Hagmann, P. Structural connectomics in brain diseases. *Neuroimage* **2013**, *80*, 515–526. [[CrossRef](#)]

33. Sporns, O. Network attributes for segregation and integration in the human brain. *Curr. Opin. Neurobiol.* **2013**, *23*, 162–171. [[CrossRef](#)]
34. Bullmore, E.T.; Bassett, D.S. Brain graphs: Graphical models of the human brain connectome. *Annu. Rev. Clin. Psychol.* **2011**, *7*, 113–140. [[CrossRef](#)]
35. Fornito, A.; Zalesky, A.; Breakspear, M. Graph analysis of the human connectome: Promise, progress, and pitfalls. *Neuroimage* **2013**, *80*, 426–444. [[CrossRef](#)]
36. Hagmann, P.; Kurant, M.; Gigandet, X.; Thiran, P.; Wedeen, V.J.; Meuli, R.; Thiran, J.P. Mapping human whole-brain structural networks with diffusion MRI. *PLoS ONE* **2007**, *2*, e597. [[CrossRef](#)]
37. Bellinger, D.C.; Jonas, R.A.; Rappaport, L.A.; Wypij, D.; Wernovsky, G.; Kuban, K.C.; Barnes, P.D.; Holmes, G.L.; Hickey, P.R.; Strand, R.D.; et al. Developmental and neurologic status of children after heart surgery with hypothermic circulatory arrest or low-flow cardiopulmonary bypass. *N. Engl. J. Med.* **1995**, *332*, 549–555. [[CrossRef](#)]
38. Bellinger, D.C.; Newburger, J.W.; Wypij, D.; Kuban, K.C.; du Plessis, A.J.; Rappaport, L.A. Behaviour at eight years in children with surgically corrected transposition: The Boston Circulatory Arrest Trial. *Cardiol. Young* **2009**, *19*, 86–97. [[CrossRef](#)]
39. Bellinger, D.C.; Wypij, D.; du Plessis, A.J.; Rappaport, L.A.; Jonas, R.A.; Wernovsky, G.; Newburger, J.W. Neurodevelopmental status at eight years in children with dextro-transposition of the great arteries: The Boston Circulatory Arrest Trial. *J. Thorac. Cardiovasc. Surg.* **2003**, *126*, 1385–1396. [[CrossRef](#)]
40. Bellinger, D.C.; Wypij, D.; Rivkin, M.J.; DeMaso, D.R.; Robertson, R.L., Jr.; Dunbar-Masterson, C.; Rappaport, L.A.; Wernovsky, G.; Jonas, R.A.; Newburger, J.W. Adolescents with d-transposition of the great arteries corrected with the arterial switch procedure: Neuropsychological assessment and structural brain imaging. *Circulation* **2011**, *124*, 1361–1369. [[CrossRef](#)]
41. Bhroin, M.N.; Seada, S.A.; Bonthron, A.F.; Kelly, C.J.; Christiaens, D.; Schuh, A.; Pietsch, M.; Hutter, J.; Tournier, J.-D.; Cordero-Grande, L. Reduced structural connectivity in cortico-striatal-thalamic network in neonates with congenital heart disease. *NeuroImage Clin.* **2020**, *28*, 102423. [[CrossRef](#)] [[PubMed](#)]
42. Feldmann, M.; Guo, T.; Miller, S.P.; Knirsch, W.; Kottke, R.; Hagmann, C.; Latal, B.; Jakab, A. Delayed maturation of the structural brain connectome in neonates with congenital heart disease. *Brain Commun.* **2020**, *2*, fcaa209. [[CrossRef](#)] [[PubMed](#)]
43. Ji, W.; Ferdman, D.; Copel, J.; Scheinost, D.; Shabanova, V.; Brueckner, M.; Khokha, M.K.; Ment, L.R. De novo damaging variants associated with congenital heart diseases contribute to the connectome. *Sci. Rep.* **2020**, *10*, 1–11. [[CrossRef](#)] [[PubMed](#)]
44. Ramirez, A.; Peyvandi, S.; Cox, S.; Gano, D.; Xu, D.; Tymofiyeva, O.; McQuillen, P.S. Neonatal brain injury influences structural connectivity and childhood functional outcomes. *PLoS ONE* **2022**, *17*, e0262310. [[CrossRef](#)]
45. Schmithorst, V.J.; Votava-Smith, J.K.; Tran, N.; Kim, R.; Lee, V.; Ceschin, R.; Lai, H.; Johnson, J.A.; De Toledo, J.S.; Blüml, S. Structural network topology correlates of microstructural brain dysmaturation in term infants with congenital heart disease. *Hum. Brain Mapp.* **2018**, *39*, 4593–4610. [[CrossRef](#)]
46. Panigrahy, A.; Schmithorst, V.J.; Wisnowski, J.L.; Watson, C.G.; Bellinger, D.C.; Newburger, J.W.; Rivkin, M.J. Relationship of white matter network topology and cognitive outcome in adolescents with d-transposition of the great arteries. *Neuroimage Clin.* **2015**, *7*, 438–448. [[CrossRef](#)]
47. Goldberg, C.S.; Gaynor, J.W.; Mahle, W.T.; Ravishankar, C.; Frommelt, P.; Iardi, D.; Bellinger, D.; Paridon, S.; Taylor, M.; Hill, K.D. The pediatric heart network’s study on long-term outcomes of children with HLHS and the impact of Norwood Shunt type in the single ventricle reconstruction trial cohort (SVRIII): Design and adaptations. *Am. Heart J.* **2022**, *254*, 216–227. [[CrossRef](#)]
48. Hagmann, P.; Cammoun, L.; Gigandet, X.; Gerhard, S.; Ellen Grant, P.; Wedeen, V.; Meuli, R.; Thiran, J.-P.; Honey, C.J.; Sporns, O. MR connectomics: Principles and challenges. *J. Neurosci. Methods* **2010**, *194*, 34–45. [[CrossRef](#)]
49. Hagmann, P.; Cammoun, L.; Gigandet, X.; Meuli, R.; Honey, C.J.; Wedeen, V.J.; Sporns, O. Mapping the structural core of human cerebral cortex. *PLoS Biol.* **2008**, *6*, e159. [[CrossRef](#)]
50. Cheng, H.; Wang, Y.; Sheng, J.; Kronenberger, W.G.; Mathews, V.P.; Hummer, T.A.; Saykin, A.J. Characteristics and variability of structural networks derived from diffusion tensor imaging. *Neuroimage* **2012**, *61*, 1153–1164. [[CrossRef](#)]
51. Achard, S.; Salvador, R.; Whitcher, B.; Suckling, J.; Bullmore, E. A resilient, low-frequency, small-world human brain functional network with highly connected association cortical hubs. *J. Neurosci.* **2006**, *26*, 63–72. [[CrossRef](#)]
52. Biswal, B.; Zerrin Yetkin, F.; Haughton, V.M.; Hyde, J.S. Functional connectivity in the motor cortex of resting human brain using echo-planar mri. *Magn. Reson. Med.* **1995**, *34*, 537–541. [[CrossRef](#)]
53. Cordes, D.; Haughton, V.M.; Arfanakis, K.; Carew, J.D.; Turski, P.A.; Moritz, C.H.; Quigley, M.A.; Meyerand, M.E. Frequencies contributing to functional connectivity in the cerebral cortex in “resting-state” data. *Am. J. Neuroradiol.* **2001**, *22*, 1326–1333.
54. Cordes, D.; Haughton, V.M.; Arfanakis, K.; Wendt, G.J.; Turski, P.A.; Moritz, C.H.; Quigley, M.A.; Meyerand, M.E. Mapping functionally related regions of brain with functional connectivity MR imaging. *Am. J. Neuroradiol.* **2000**, *21*, 1636–1644.
55. Lowe, M.; Mock, B.; Sorenson, J. Functional connectivity in single and multislice echoplanar imaging using resting-state fluctuations. *Neuroimage* **1998**, *7*, 119–132. [[CrossRef](#)]
56. Casey, B.J.; Cannonier, T.; Conley, M.I.; Cohen, A.O.; Barch, D.M.; Heitzeg, M.M.; Soules, M.E.; Teslovich, T.; Dellarco, D.V.; Garavan, H. The adolescent brain cognitive development (ABCD) study: Imaging acquisition across 21 sites. *Dev. Cogn. Neurosci.* **2018**, *32*, 43–54. [[CrossRef](#)]
57. Owen, J.P.; Ziv, E.; Bukshpun, P.; Pojman, N.; Wakahiro, M.; Berman, J.I.; Roberts, T.P.; Friedman, E.J.; Sherr, E.H.; Mukherjee, P. Test–Retest Reliability of Computational Network Measurements Derived from the Structural Connectome of the Human Brain. *Brain Connect.* **2013**, *3*, 160–176. [[CrossRef](#)]

58. Walker, L.; Curry, M.; Nayak, A.; Lange, N.; Pierpaoli, C. A framework for the analysis of phantom data in multicenter diffusion tensor imaging studies. *Hum. Brain Mapp.* **2013**, *34*, 2439–2454. [[CrossRef](#)]
59. Mulkern, R.V.; Forbes, P.; Dewey, K.; Osganian, S.; Clark, M.; Wong, S.; Ramamurthy, U.; Kun, L.; Poussaint, T.Y. Establishment and Results of a Magnetic Resonance Quality Assurance Program for the Pediatric Brain Tumor Consortium. *Acad. Radiol.* **2008**, *15*, 1099–1110. [[CrossRef](#)]
60. Poussaint, T.Y.; Phillips, P.C.; Vajapeyam, S.; Fahey, F.H.; Robertson, R.L.; Osganian, S.; Ramamurthy, U.; Mulkern, R.V.; Treves, S.T.; Boyett, J.M.; et al. The Neuroimaging Center of the Pediatric Brain Tumor Consortium—collaborative neuroimaging in pediatric brain tumor research: A work in progress. *AJNR Am. J. Neuroradiol.* **2007**, *28*, 603–607.
61. Marcus, D.S.; Harms, M.P.; Snyder, A.Z.; Jenkinson, M.; Wilson, J.A.; Glasser, M.F.; Barch, D.M.; Archie, K.A.; Burgess, G.C.; Ramaratnam, M.; et al. Human Connectome Project informatics: Quality control, database services, and data visualization. *Neuroimage* **2013**, *80*, 202–219. [[CrossRef](#)] [[PubMed](#)]
62. Elam, J.S.; Van Essen, D. *Human Connectome Project, Encyclopedia of Computational Neuroscience*; Springer: Berlin/Heidelberg, Germany, 2014; pp. 1–4.
63. Sotiropoulos, S.N.; Jbabdi, S.; Xu, J.; Andersson, J.L.; Moeller, S.; Auerbach, E.J.; Glasser, M.F.; Hernandez, M.; Sapiro, G.; Jenkinson, M. Advances in diffusion MRI acquisition and processing in the Human Connectome Project. *Neuroimage* **2013**, *80*, 125–143. [[CrossRef](#)] [[PubMed](#)]
64. Van Essen, D.C.; Smith, S.M.; Barch, D.M.; Behrens, T.E.; Yacoub, E.; Ugurbil, K. The WU-Minn human connectome project: An overview. *Neuroimage* **2013**, *80*, 62–79. [[CrossRef](#)] [[PubMed](#)]
65. Zuo, X.-N.; Xing, X.-X. Test-retest reliabilities of resting-state fMRI measurements in human brain functional connectomics: A systems neuroscience perspective. *Neurosci. Biobehav. Rev.* **2014**, *45*, 100–118. [[CrossRef](#)]
66. Dams-O'Connor, K.; Spielman, L.; Singh, A.; Gordon, W.A.; Lingsma, H.F.; Maas, A.I.; Manley, G.T.; Mukherjee, P.; Okonkwo, D.O.; Puccio, A.M. The Impact of Previous Traumatic Brain Injury on Health and Functioning: A TRACK-TBI Study. *J. Neurotrauma* **2013**, *30*, 2014–2020. [[CrossRef](#)]
67. Yue, J.K.; Vassar, M.J.; Lingsma, H.F.; Cooper, S.R.; Okonkwo, D.O.; Valadka, A.B.; Gordon, W.A.; Maas, A.I.; Mukherjee, P.; Yuh, E.L. Transforming research and clinical knowledge in traumatic brain injury pilot: Multicenter implementation of the common data elements for traumatic brain injury. *J. Neurotrauma* **2013**, *30*, 1831–1844. [[CrossRef](#)]
68. Yuh, E.L.; Cooper, S.R.; Mukherjee, P.; Yue, J.K.; Lingsma, H.; Gordon, W.; Valadka, A.; Okonkwo, D.O.; Schnyer, D.M.; Vassar, M.J. Diffusion Tensor Imaging for Outcome Prediction in Mild Traumatic Brain Injury: A TRACK-TBI Study. *J. Neurotrauma* **2014**, *31*, 1457–1477. [[CrossRef](#)]
69. Keenan, K. Quantitative Magnetic Resonance Imaging and Phantom Development. *Bull. Am. Phys. Soc.* **2014**, *59*, Y38-001.
70. Selwyn, R. *Phantoms for Magnetic Resonance Imaging, The Phantoms of Medical and Health Physics*; Springer: Berlin/Heidelberg, Germany, 2014; pp. 181–199.
71. Vannier, M.W. *Traumatic Brain Injury Diffusion Magnetic Resonance Imaging Research Roadmap Development Project*; DTIC Document; Chicago University: Chicago, IL, USA, 2010.
72. Glover, G.H.; Mueller, B.A.; Turner, J.A.; van Erp, T.G.; Liu, T.T.; Greve, D.N.; Voyvodic, J.T.; Rasmussen, J.; Brown, G.G.; Keator, D.B. Function biomedical informatics research network recommendations for prospective multicenter functional MRI studies. *J. Magn. Reson. Imaging* **2012**, *36*, 39–54. [[CrossRef](#)]
73. Friedman, L.; Glover, G.H. Report on a multicenter fMRI quality assurance protocol. *J. Magn. Reson. Imaging* **2006**, *23*, 827–839. [[CrossRef](#)]
74. Friedman, L.; Glover, G.H.; Consortium, F. Reducing interscanner variability of activation in a multicenter fMRI study: Controlling for signal-to-fluctuation-noise-ratio (SFNR) differences. *Neuroimage* **2006**, *33*, 471–481. [[CrossRef](#)]
75. Friedman, L.; Glover, G.H.; Krenz, D.; Magnotta, V. Reducing inter-scanner variability of activation in a multicenter fMRI study: Role of smoothness equalization. *Neuroimage* **2006**, *32*, 1656–1668. [[CrossRef](#)]
76. Friedman, L.; Stern, H.; Brown, G.G.; Mathalon, D.H.; Turner, J.; Glover, G.H.; Gollub, R.L.; Lauriello, J.; Lim, K.O.; Cannon, T. Test-retest and between-site reliability in a multicenter fMRI study. *Hum. Brain Mapp.* **2008**, *29*, 958–972. [[CrossRef](#)]
77. Keator, D.B.; Grethe, J.S.; Marcus, D.; Ozyurt, B.; Gadde, S.; Murphy, S.; Pieper, S.; Greve, D.; Notestine, R.; Bockholt, H.J. A national human neuroimaging collaboratory enabled by the Biomedical Informatics Research Network (BIRN). *Inf. Technol. Biomed. IEEE Trans.* **2008**, *12*, 162–172. [[CrossRef](#)]
78. Marcus, D.S.; Harwell, J.; Olsen, T.; Hodge, M.; Glasser, M.F.; Prior, F.; Jenkinson, M.; Laumann, T.; Curtiss, S.W.; Van Essen, D.C. Informatics and data mining tools and strategies for the human connectome project. *Front. Neuroinform.* **2011**, *5*, 4. [[CrossRef](#)]
79. Marcus, D.S.; Olsen, T.R.; Ramaratnam, M.; Buckner, R.L. The extensible neuroimaging archive toolkit. *Neuroinformatics* **2007**, *5*, 11–33. [[CrossRef](#)]
80. Haldar, J.P.; Leahy, R.M. Linear transforms for Fourier data on the sphere: Application to high angular resolution diffusion MRI of the brain. *Neuroimage* **2013**, *71*, 233–247. [[CrossRef](#)]
81. Shattuck, D.W.; Prasad, G.; Mirza, M.; Narr, K.L.; Toga, A.W. Online resource for validation of brain segmentation methods. *Neuroimage* **2009**, *45*, 431–439. [[CrossRef](#)]
82. Shattuck, D.W.; Leahy, R.M. BrainSuite: An automated cortical surface identification tool. *Med. Image Anal.* **2002**, *6*, 129–142. [[CrossRef](#)]

83. Joshi, A.A.; Pantazis, D.; Li, Q.; Damasio, H.; Shattuck, D.W.; Toga, A.W.; Leahy, R.M. Sulcal set optimization for cortical surface registration. *Neuroimage* **2010**, *50*, 950–959. [[CrossRef](#)]
84. Fennema-Notestine, C.; Ozyurt, I.B.; Clark, C.P.; Morris, S.; Bischoff-Grethe, A.; Bondi, M.W.; Jernigan, T.L.; Fischl, B.; Segonne, F.; Shattuck, D.W.; et al. Quantitative evaluation of automated skull-stripping methods applied to contemporary and legacy images: Effects of diagnosis, bias correction, and slice location. *Hum. Brain Mapp.* **2006**, *27*, 99–113. [[CrossRef](#)] [[PubMed](#)]
85. Joshi, A.A.; Shattuck, D.W.; Thompson, P.M.; Leahy, R.M. Surface-constrained volumetric brain registration using harmonic mappings. *Med. Imaging IEEE Trans.* **2007**, *26*, 1657–1669. [[CrossRef](#)] [[PubMed](#)]
86. Joshi, A.A.; Shattuck, D.W.; Thompson, P.M.; Leahy, R.M. A parameterization-based numerical method for isotropic and anisotropic diffusion smoothing on non-flat surfaces. *Image Process. IEEE Trans.* **2009**, *18*, 1358–1365. [[CrossRef](#)] [[PubMed](#)]
87. Pantazis, D.; Joshi, A.; Jiang, J.; Shattuck, D.W.; Bernstein, L.E.; Damasio, H.; Leahy, R.M. Comparison of landmark-based and automatic methods for cortical surface registration. *Neuroimage* **2010**, *49*, 2479–2493. [[CrossRef](#)]
88. Malykhin, N.; Concha, L.; Seres, P.; Beaulieu, C.; Coupland, N.J. Diffusion tensor imaging tractography and reliability analysis for limbic and paralimbic white matter tracts. *Psychiatry Res. Neuroimaging* **2008**, *164*, 132–142. [[CrossRef](#)]
89. Jiang, H.; van Zijl, P.; Kim, J.; Pearlson, G.D.; Mori, S. DtiStudio: Resource program for diffusion tensor computation and fiber bundle tracking. *Comput. Methods Programs Biomed.* **2006**, *81*, 106–116. [[CrossRef](#)]
90. Yeh, F.-C.; Wedeen, V.J.; Tseng, W.-Y.I. Estimation of fiber orientation and spin density distribution by diffusion deconvolution. *Neuroimage* **2011**, *55*, 1054–1062. [[CrossRef](#)]
91. Power, J.D.; Mitra, A.; Laumann, T.O.; Snyder, A.Z.; Schlaggar, B.L.; Petersen, S.E. Methods to detect, characterize, and remove motion artifact in resting state fMRI. *Neuroimage* **2014**, *84*, 320–341. [[CrossRef](#)]
92. Yan, C.-G.; Craddock, R.C.; He, Y.; Milham, M.P. Addressing head motion dependencies for small-world topologies in functional connectomics. *Front. Hum. Neurosci.* **2013**, *7*, 910. [[CrossRef](#)]
93. Achard, S.; Bullmore, E. Efficiency and cost of economical brain functional networks. *PLoS Comput. Biol.* **2007**, *3*, e17. [[CrossRef](#)]
94. Xia, M.; Wang, J.; He, Y. BrainNet Viewer: A network visualization tool for human brain connectomics. *PLoS ONE* **2013**, *8*, e68910. [[CrossRef](#)]
95. Rubinov, M.; Sporns, O. Complex network measures of brain connectivity: Uses and interpretations. *Neuroimage* **2010**, *52*, 1059–1069. [[CrossRef](#)]
96. Ginestet, C.E.; Nichols, T.E.; Bullmore, E.T.; Simmons, A. Brain network analysis: Separating cost from topology using cost-integration. *PLoS ONE* **2011**, *6*, e21570. [[CrossRef](#)]
97. Fruchterman, T.M.; Reingold, E.M. Graph drawing by force-directed placement. *Softw. Pract. Exp.* **1991**, *21*, 1129–1164. [[CrossRef](#)]
98. Krzywinski, M.; Schein, J.; Birol, I.; Connors, J.; Gascoyne, R.; Horsman, D.; Jones, S.J.; Marra, M.A. Circos: An information aesthetic for comparative genomics. *Genome Res.* **2009**, *19*, 1639–1645. [[CrossRef](#)]
99. Schmithorst, V.J.; Badaly, D.; Beers, S.R.; Lee, V.K.; Weinberg, J.; Lo, C.W.; Panigrahy, A. *Relationships between Regional Cerebral Blood Flow and Neurocognitive Outcomes in Children and Adolescents with Congenital Heart Disease, Seminars in Thoracic and Cardiovascular Surgery*; Elsevier: Amsterdam, The Netherlands, 2021; Volume 34, pp. 1285–1295.
100. DiCiccio, T.J.; Efron, B. Bootstrap Confidence Intervals. *Stat. Sci.* **1996**, *11*, 189–228. [[CrossRef](#)]
101. Hayes, A.F.; Scharkow, M. The relative trustworthiness of inferential tests of the indirect effect in statistical mediation analysis: Does method really matter? *Psychol. Sci.* **2013**, *24*, 1918–1927. [[CrossRef](#)]
102. Benjamini, Y.; Hochberg, Y. On the Adaptive Control of the False Discovery Rate in Multiple Testing with Independent Statistics. *J. Educ. Behav. Stat.* **2000**, *25*, 60–83. [[CrossRef](#)]
103. Meyers, B.D.; Lee, V.K.; Dennis, L.G.; Wallace, J.; Schmithorst, V.; Votava-Smith, J.K.; Rajagopalan, V.; Herrup, E.; Baust, T.; Tran, N.N. Harmonization of Multi-Center Diffusion Tensor Tractography in Neonates with Congenital Heart Disease: Optimizing Post-Processing and Application of ComBat. *Neuroimage Rep.* **2022**, *2*, 100114. [[CrossRef](#)]

Disclaimer/Publisher’s Note: The statements, opinions and data contained in all publications are solely those of the individual author(s) and contributor(s) and not of MDPI and/or the editor(s). MDPI and/or the editor(s) disclaim responsibility for any injury to people or property resulting from any ideas, methods, instructions or products referred to in the content.